RSC Advances

PAPER

View Article Online
View Journal | View Issue

Cite this: *RSC Adv.*, 2020, **10**, 11046

Two rare $\{M_2(MoO_4)_2\}_n$ chain-containing molybdate-based metal–organic complexes with a bis-pyrazole-bis-amide ligand: fluorescent sensing and photocatalysis performance†

Xiuli Wang, ‡* Xiang Pan,‡ Xiang Wang,* Yan Li and Guocheng Liu

Received 14th February 2020
Accepted 11th March 2020

DOI: 10.1039/d0ra01420f

rsc.li/rsc-advances

By introducing a bis-pyrazole-bis-amide ligand, *N*,*N*′-bis(1*H*-pyrazole-4-carboxamide)-1,4-benzene (L), two molybdate-based metal–organic complexes containing $\{M_2(MoO_4)_2\}_n$ (M = Co, Zn), $[Co_2L_2(MoO_4)_2]\cdot H_2O$ (**1**), $[Zn_2L_2(MoO_4)_2]\cdot H_2O$ (**2**), have been prepared under hydrothermal/solvothermal conditions. X-ray diffraction analyses reveal that both **1** and **2** are isostructural. An interesting structural feature is that a kind of $\{M_2(MoO_4)_2\}_n$ chain could be found in **1** and **2**, although different raw materials $[Mo_7O_{24}]^{6-}$ and $[PMo_{12}O_{40}]^{3-}$ anions were utilized. Then these chains are further linked by L ligands into a two dimensional (2D) structure. The title complexes represent the first examples containing $\{MoO_4\}$ units and pyrazole-/or amide-derivative ligands. Complexes **1** and **2** exhibit distinct performances due to different metal centers, with **2** acting as a fluorescent sensor for Fe^{3+}, MnO_4^-, CrO_4^{2-} and $Cr_2O_7^{2-}$, but **1** being a better photocatalyst towards degradation of cationic dyes methylene blue (MB) and neutral red (NR).

Introduction

Currently, as an important research branch of polyoxometalate (POM) chemistry, polyoxomolybdate-based metal–organic complexes (MOCs) have attracted numerous researchers' attention, not only due to their diverse structures caused by different amounts of molybdenum centers,[1–7] but also their outstanding properties in the fields of electrochemistry, medicine, fluorescence, materials and photocatalysis, *et al.*[8,9] During the synthesis of these MOCs, the polyoxomolybdates, including $[MoO_4]^{2-}$, $[Mo_3O_{10}]^{2-}$, $[Mo_7O_{24}]^{6-}$, $[Mo_8O_{26}]^{4-}$ and so on,[10–13] can be usually produced by changing reaction conditions or raw materials. Among them, the $\{MoO_4\}$ unit-containing MOCs are of interest, which can be converted from different raw materials.[14] However, reports on the $\{MoO_4\}$-based MOCs are still very limited. In 1998, Zubieta's group synthesized a Cu-based complex [Cu(dpe)(MoO$_4$)] (dpe = 1,2-*trans*-(4-pyridyl)ethane),[15] where the $[MoO_4]^{2-}$ unit was derived from a MoO_3 raw material. The same Zubieta's group used Ni^{II}, di-4-pyridylamine (dpa) ligand and appropriate oxides (Et_4NOH) to produce a Ni^{II}-organic diamine-EO_4^{2-} (E = S or Mo) complex $[Ni(dpa)_2(MoO_4)]$ through hydrothermal reaction in 1999.[16] Using $Na_2MoO_4\cdot 2H_2O$ as a raw material, a complex $[Cu(4,4'\text{-bpy})]_2[MoO_4]\cdot 2H_2O$ containing $[MoO_4]^{2-}$ units was obtained by Huang's group.[17] In complex $[Zn_2(H_2O)L(MoO_4)]_n$ (L = 2,2′-bipyridine-6,6′-dicarboxylic acid) prepared by Niu's group in 2011, the $[MoO_4]^{2-}$ unit came of $Na_2H[PMo_{12}O_{40}]\cdot 14H_2O$.[18] In addition, some inorganic functional materials constructed with $\{MoO_4\}$ units and metals have also been reported, which have a wide range of applications.[19,20] However, as mentioned above, most of the $[MoO_4]^{2-}$-containing MOCs are constructed from pyridyl derivated ligands, the use of pyrazole-/or amide-derivative ligands in the preparing molybdate-based MOCs has not been reported yet.

Here, we try to introduce bis-pyrazole-bis-amide ligand, *N*,*N*′-bis(1*H*-pyrazole-4-carboxamide)-1,4-benzene (L) (Scheme 1) into the reaction system containing $[Mo_7O_{24}]^{6-}$ and $[PMo_{12}O_{40}]^{3-}$ anions to synthesize POM-based cobalt(II) or zinc(II) complexes. Fortunately, two isomorphic MOCs $[Co_2L_2(MoO_4)_2]\cdot H_2O$ (**1**) and $[Zn_2L_2(MoO_4)_2]\cdot H_2O$ (**2**) were obtained under different reaction conditions, both of which consist of a kind of rare $\{M_2(MoO_4)_2\}_n$ chain and L ligands. To the best of our knowledge, the title

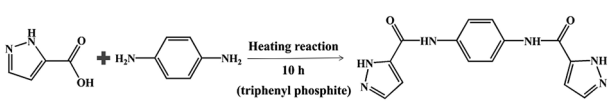

Scheme 1 The synthesis process of the ligand L in this work.

College of Chemistry and Chemical Engineering, Professional Technology Innovation Center of Liaoning Province for Conversion Materials of Solar Cell, Bohai University, Jinzhou 121013, P. R. China. E-mail: wangxiuli@bhu.edu.cn; wx_2007@163.com ; Fax: +86 416 3400158; Tel: +86 416 3400158

† Electronic supplementary information (ESI) available: IR, PXRD and additional figures. CCDC supplementary crystallographic data for the two molybdate-based metal–organic complexes synthesized in this article, numbered 1972119 and 1972120. For ESI and crystallographic data in CIF or other electronic format see DOI: 10.1039/d0ra01420f

‡ These authors contributed equally to this work.

complexes represent the first examples of MOCs combining MoO_4^{2-} units and pyrazole-/or amide-derivative ligands, especially using different molybdate-containing raw materials. The fluorescence and photocatalytic properties of complexes **1** and **2** were investigated further.

Experimental

Materials and methods

All chemicals and solvents were purchased from commercial sources, and used without further purification before the experiment. The synthesis method of ligand L was obtained according to previous literature.[21] The FT-IR spectra were collected on a Varian 640 FT-IR spectrometer. Powder X-ray diffraction (PXRD) data were taken on a D/teX Ultra diffractometer by Cu Kα radiation. The collection of fluorescence experimental data was obtained by using Hitachi F-4500 fluorescence spectrometer. A diffuse reflectivity spectrum were collected with a spectrophotometer (Lambda, Model 750). The UV-vis absorption spectra was measured by a SP-1901 UV-vis spectrophotometer.

Synthesis of complexes 1–2

Synthesis of $[Co_2L_2(MoO_4)_2]\cdot H_2O$ (1). A mixture of $CoCl_2\cdot 6H_2O$ (0.048 g, 0.2 mmol), L (0.025 g, 0.1 mmol), $(NH_4)_6Mo_7O_{24}\cdot 4H_2O$ (0.124 g, 0.1 mmol) in a mixed-solvent of 6 mL water and 4 mL DMF (*N*,*N*-dimethylformamide) was transferred into a Teflon-lined autoclave and kept at 120 °C for 4 days. After slow cooling to room temperature, pink block crystals of **1** were obtained in a yield of 45% based on Co. Anal calcd for $C_{28}H_{26}Co_2Mo_2N_{12}O_{13}$ (%): C 32.08, H 2.50, N 13.03; found: C 32.01, H 2.42, N 12.98. IR (KBr pellet, cm^{-1}): 3414 (s), 3294 (w), 3119 (w), 2354 (w), 1628 (s), 1540 (s), 1409 (w), 1340 (s), 1246 (m), 1183 (w), 1114 (m), 1064 (m), 1007 (m), 914 (m), 870 (m), 832 (w), 763 (m), 682 (m), 644 (w), 600 (w).

Synthesis of $[Zn_2L_2(MoO_4)_2]\cdot H_2O$ (2). A mixture of $ZnNO_3\cdot 6H_2O$ (0.060 g, 0.2 mmol), L (0.025 g, 0.1 mmol), $H_3PMo_{12}O_{40}\cdot 12H_2O$ (0.183 g, 0.1 mmol) in a mixed-solvent of 6 mL water and 4 mL NaOH (0.1 mol L^{-1}) was transferred into a Teflon-lined autoclave and kept at 120 °C for 4 days. After slow cooling to room temperature, yellow block crystals of **2** were obtained in a yield of 28% based on Zn. Anal calcd for $C_{28}H_{26}Zn_2Mo_2N_{12}O_{13}$ (%): C 31.69, H 2.47, N 15.84; found: C 31.62, H 2.41, N 15.78. IR (KBr pellet, cm^{-1}): 3395 (w), 3289 (w), 3119 (w), 2361 (w), 1641 (s), 1540 (s), 1459 (w), 1409 (w), 1371 (w), 1340 (s), 1283 (w), 1252 (m), 1177 (w), 1114 (m), 1064 (w), 1007 (w), 870 (s), 776 (m), 694 (w), 650 (w), 600 (w).

X-ray crystallography

X-ray crystallographic data for complexes **1–2** were collected at 293 K on a Bruker SMART APEX II CCD diffractometer equipped with MoKα monochromatic radiation (λ = 0.71069 Å) by φ and ω scanning methods. The crystal structure of the title complexes was solved by direct method using SHELXTL-2014 program, and further refined on F^2 by full matrix least square method.[22] The crystallographic data and detailed parameters of complexes **1–2** reported in this paper are listed in Table 1. The selected bond length (Å) and angle (°) of complexes **1–2** are provided in Table S1.† The complexes **1–2** have been recorded at the Cambridge Crystallographic Data Center under the numbers 1972119 and 1972120.

Result and discussion

Syntheses of complexes 1 and 2

In previous reports, most $\{MoO_4\}$-based complexes were obtained from raw materials MoO_3, $Na_2MoO_4\cdot 2H_2O$ *etc.*[14,15] In this work, an interesting feature is that the raw materials $[Mo_7O_{24}]^{6-}$ and $[PMo_{12}O_{40}]^{3-}$ anions were transformed into $\{MoO_4\}$ units in final structures of complexes **1** and **2**, which have rarely been observed in previous reports. During the synthesis, we also used other raw materials, such as $Na_2MoO_4\cdot 2H_2O$ to synthesize the title complexes, however, no single crystal complexes could be obtained. In addition, for complex **1**, $[PMo_{12}O_{40}]^{3-}$ anions was also introduced into the synthesis system in place of $[Mo_7O_{24}]^{6-}$, as a result, only some precipitates could be obtained and no crystals could be formed; for complex **2**, when the Zn^{II} and $[Mo_7O_{24}]^{6-}$ are used as raw materials, and no single crystal products could be synthesized. It can be concluded that the conversion of $\{MoO_4\}$ structural units requires specific reaction conditions and raw materials. That is to say, the metals and polyoxometalate, as well as solvent system, have a significant effect on the synthesis of the target products.

Crystal structure of 1 and 2

Single crystal X-ray diffraction shows that complexes **1** and **2** are isostructural, both of which are 2D networks and belong to the

Table 1 Crystallographic data for complexes **1–2**

Complex	**1**	**2**
Empirical formula	$C_{28}H_{26}Co_2Mo_2N_{12}O_{13}$	$C_{28}H_{26}Zn_2Mo_2N_{12}O_{13}$
Formula weight	1048.35	1061.23
Temperature/K	293(2) K	293(2) K
Crystal system	Monoclinic	Monoclinic
Space group	*C*2/*c*	*C*2/*c*
a/Å	32.758(5)	32.805(4)
b/Å	6.9308(10)	7.0020(8)
c/Å	15.972(2)	15.9094(19)
α/°	90	90
β/°	113.128(5)	112.537(4)
γ/°	90	90
V/Å^3	3334.9(8)	3375.3(7)
Z	4	4
D_c (g cm^{-3})	2.088	2.088
μ/mm^{-1}	1.801	2.218
F(000)	2080	2104
Reflection collected	10 970	11 936
Unique reflections	3759	4165
Parameters	258	258
R_{int}	0.0648	0.0581
Goodness on F^2	0.991	0.943
$R_1{}^a$ [$I > 2\sigma(I)$]	0.0434	0.0383
w$R_2{}^b$ (all data)	0.0957	0.0846

^{a} $R_1 = \sum||F_o| - |F_c||/\sum|F_o|$. ^{b} $wR_2 = \{\sum[w(F_{o2} - F_{c2})_2]/\sum[w(F_{o2})_2]\}_{1/2}$.

*C*2/*c* space group in the monoclinic system. Here, only the structure of complex **1** is described in details as a representative. As shown in Fig. 1a, the asymmetric unit of **1** contains one crystallographically independent Co^{II} cation, one L ligand, one $[MoO_4]^{2-}$ anion and half of water molecule. The valence sum calculations display that the Mo atoms are in the +VI oxidation state, and the Co atom are in the +II oxidation state.[23] The Co^{II} center is six-coordinated and displays a twisted octahedral coordination geometry, surrounded by two pyrazole N atoms (N1 and N2) from two L ligands and one O atom (O1) from the amide group in the ligand, three terminal O atoms (O3, O4 and O5) belonging to three $[MoO_4]^{2-}$ anions, respectively. The bond lengths of Co–N and Co–O are in the range of 2.111(4) to 2.128(4) Å and 2.054(4) to 2.184(3) Å, respectively.

In complex **1**, each of Mo atoms is a tetrahedral configuration, surrounded by four oxygen atoms, and further aggregated by the six-coordinated Co atoms *via* sharing three oxygen atoms (O3, O4, O5) to give a $\{Co_2(MoO_4)_2\}_n$ chain (Fig. 1b). These $\{Co_2(MoO_4)_2\}_n$ chains are extended by L ligands into a 2D layer (Fig. 1c). On one hand, the L ligands acting as bridging linkers are arranged in pair and in an inverted mode. On the other hand, each of L ligands shows a tridentate coordination mode, namely, both N1 atom of pyrazolyl and O1 atom of amide at one end of L ligand chelate together one Co^{II} ion, but only one N2 atom of pyrazolyl at another end of L ligand coordinates with one Co^{II} center. In fact, each Co^{II} ion is surrounded with such two kinds of L ligands. Complex **2** also has a 2D structure, which is similar to that of complex **1**, and the corresponding structure is shown in Fig. S1.†

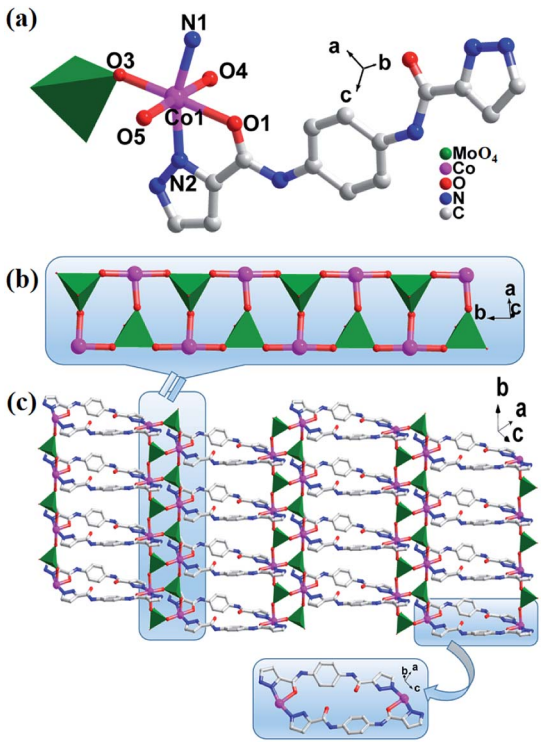

Fig. 1 (a) Ball/stick/polyhedron view of the asymmetric unit of **1**. The hydrogen atoms are omitted for clarity; (b) the view of polyoxometalate chain $\{Co/MoO_4\}_n$; (c) the 2D network structure of **1**.

PXRD and IR

As shown in Fig. S2,† the PXRD results of the complexes **1–2** at room temperature basically coincide with the simulated diffraction peaks of the complexes **1–2**, and the results show that the phase purity and stability of the complexes are good. The slight difference in intensity between the diffraction peaks may be due to the orientation of the crystallites in the powder sample tested.[24]

The IR test results of complexes **1–2** are shown in Fig. S3.† Because complexes **1** and **2** are isomorphic complexes, their infrared peak positions are generally the same, except that the peak strength is slightly different. The characteristic absorption peaks of 1064 cm^{-1} for **1** and **2** are attributed to the $\nu(Mo{=}O_t)$, but the peak intensities are different. And the ν(M–O–Mo) (M = Co or Zn) vibration peak in complexes **1–2** is at 870 cm^{-1}.[18] Bands at 1628 cm^{-1} for **1**, 1641 cm^{-1} for **2**, can be attributed to the ν(C=O), respectively. The ν(N–H) vibrations peak in complexes **1–2** is at 1409 cm^{-1}.[25] In addition, the characteristic bands from –OH groups of water molecules can be observed in the vicinity of 3414 cm^{-1} for **1**, 3395 cm^{-1} for **2**.[26]

Fluorescence properties

Generally, polyoxomolybdate-based MOCs based on Zn^{II} have shown good properties and applications as fluorescent materials.[27–29] Therefore, the solid-state fluorescent properties of complexes **1–2**, were also investigated at room temperature, as well as L, $H_3PMo_{12}O_{40}\cdot 12H_2O$ and $(NH_4)_6Mo_7O_{24}\cdot 4H_2O$. As shown in Fig. 2a, the free L ligand shows strong emission band at 401 nm (λ_{ex} = 300 nm), such transitions are $\pi^* \rightarrow \pi$ in nature.[30] As we expected, only the emission spectrum of complex **2** based on Zn^{II} ion is observed at approximately 428 nm (λ_{ex} = 300 nm), and the similarity to the free L ligand may be owing to the intraligand transition of the ligands.[31,32] However, complex **1**, $H_3PMo_{12}O_{40}\cdot 12H_2O$ and $(NH_4)_6Mo_7O_{24}\cdot 4H_2O$ have no obvious emission peaks, compared to that of complex **2**.

In general, hydrothermally or solvothermally synthesized complexes have good stability. In this work, complex **2** is insoluble in water and other salt solutions. Therefore, its abilities to detect metal cations in aqueous solution were explored. As shown in Fig. 2b, the fluorescence response experiments of complex **2** containing different metal cations with 10^{-3} M (Na^+, K^+, Hg^{2+}, Ni^{2+}, Mg^{2+}, Cu^{2+}, Co^{2+}, Gd^{3+}, Nd^{3+} and Fe^{3+}) were performed.[33] It can be observed clearly that the fluorescence intensity of the suspension of complex **2** containing only Fe^{3+} ions is significantly quenched. In comparison, other metal cations have no significant effect on the emission intensity. The results indicate that complex **2** may have a good ability to fluorescence detect Fe^{3+} ion in aqueous solutions. Thus, the anti-interference experiments were also studied. Fig. 2c shows that the fluorescence quenching activities of suspensions in the presence of other cations can be still observed with the addition of Fe^{3+} ions, confirms that complex **2** has a high selectivity for detecting Fe^{3+} ions.

In order to further explore the sensitivity of complex **2** to detect Fe^{3+} ions, the quantitative fluorescence titration experiment was performed. As shown in Fig. 2d, with the quantitative addition of Fe^{3+} ions (concentration changed from 0 to 10^{-3} M), the emission intensity of the suspension of complex **2** are

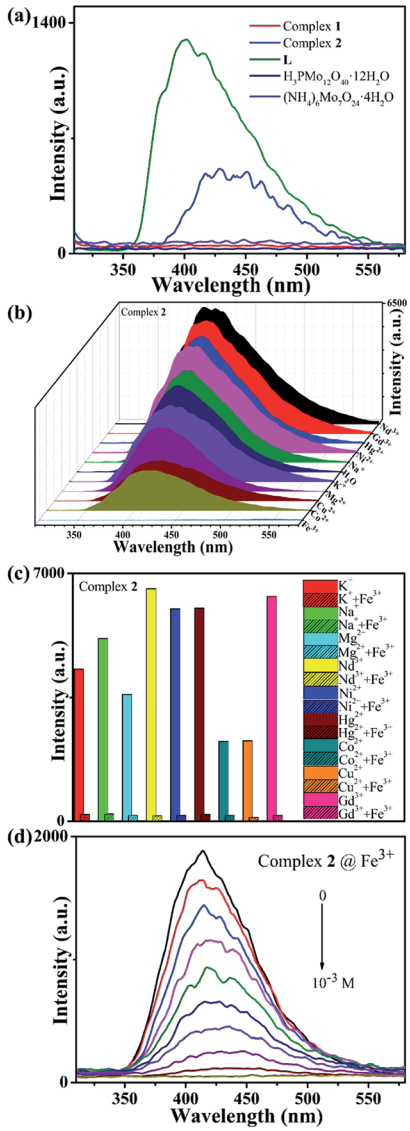

Fig. 2 (a) Fluorescence spectra of complexes 1–2, L, $H_3PMo_{12}O_{40}\cdot 12H_2O$ and $(NH_4)_6Mo_7O_{24}\cdot 4H_2O$ at solid state; (b) fluorescence spectra of M^{n+} @ 2; (c) fluorescence emission intensities of 2 at room temperature upon the addition of Fe^{3+} or Fe^{3+} + M^{n+} ions; (d) emission spectra of the suspension of 2 with the Fe^{3+} aqueous concentration from 0 to 10^{-3} M.

weakened gradually, and the fluorescence quenching efficiency reaches to as high as 99.1% (Fig. S4†). Based on the good linear relationship at lower concentrations between the fluorescence intensity and the concentration of Fe^{3+} ions, the Stern–Volmer equation ($I_0/I = 1 + K_{SV}[C]$) is used to describe the fluorescence quenching effect,[34] where K_{SV} is the quenching constant (M^{-1}), [C] is Fe^{3+} ions concentration, I_0 and I are the emission intensities before and after Fe^{3+} ions were added. As shown in Fig. S5,† the K_{SV} value of Fe^{3+} is calculated as 2.53×10^4 M^{-1}. The results indicate that complex 2 has excellent sensitivity to detect Fe^{3+} ions in aqueous solution.

Further, different anions including Br^-, NO_2^-, Cl^-, OH^-, I^-, Ac^-, MnO_4^-, CrO_4^{2-}, $Cr_2O_7^{2-}$, were selected to explore the fluorescence detection abilities for anions of complex 2. The experiment method was similar to that of cation involved. As shown in Fig. 3a, when the MnO_4^-, CrO_4^{2-} or $Cr_2O_7^{2-}$ anions are added, the emission peak of the suspension containing complex 2 undergoes significant quenching behaviours, while the fluorescence intensities have only slight changes for other anions. When the MnO_4^- (CrO_4^{2-} and $Cr_2O_7^{2-}$) anion is added to suspension of complex 2 containing other anions, the fluorescence intensity of the suspension can still be effectively

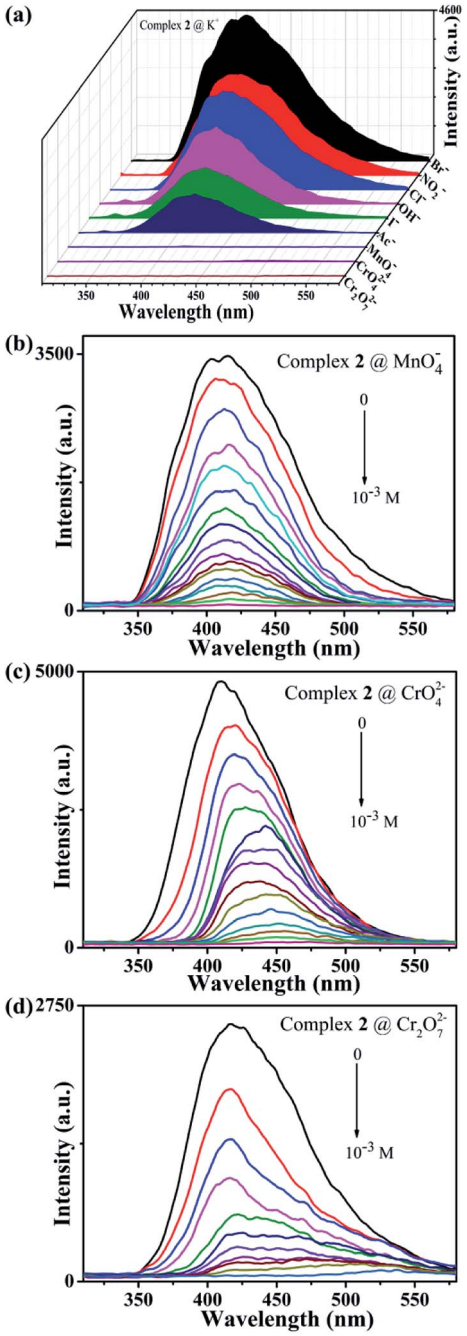

Fig. 3 (a) Fluorescence spectra of 2 immersed into aqueous solution containing various anions; (b) fluorescence spectra of quantitatively titrating the MnO_4^{2-}, (c) CrO_4^{2-} and (d) $Cr_2O_7^{2-}$ anion aqueous solution into the suspension of complex 2 (concentration range is from 0 to 10^{-3} M).

quenched, indicating that complex **2** has high selectivity for fluorescence detection MnO_4^- (CrO_4^{2-} and $Cr_2O_7^{2-}$) anion (Fig. S6†). In addition, we quantitatively added MnO_4^- (CrO_4^{2-} and $Cr_2O_7^{2-}$) anion aqueous solution to the suspension of complex **2** at a concentration from 0 to 10^{-3} M. As shown in Fig. 3b–d, as the MnO_4^- (CrO_4^{2-} and $Cr_2O_7^{2-}$) anion is quantitatively increased, the fluorescence intensity of the mixture suspension gradually decreases until it is completely quenched, which proves that complex **2** has good sensitivity for fluorescence detection of MnO_4^- (CrO_4^{2-} and $Cr_2O_7^{2-}$) anion aqueous solution. The K_{SV} values of 1.97×10^4 M^{-1} (MnO_4^-) and 2.31×10^4 M^{-1} (CrO_4^{2-}) show strong quenching effects on these anions for complex **2**, while the fluorescence intensity has an exponential relationship with the concentration of $Cr_2O_7^{2-}$ anion at lower concentrations (Fig. S5†). Meanwhile, the fluorescence quenching efficiency is as high as 99.3% for MnO_4^-, 99.2% for CrO_4^{2-}, 99.4% for $Cr_2O_7^{2-}$, respectively (Fig. S4†).

Furthermore, the quenching mechanism was explored to understand the quenching effect of complex **2** on Fe^{3+}, MnO_4^-, CrO_4^{2-} and $Cr_2O_7^{2-}$ ions. Firstly, after being immersed in these ions aqueous solution for 24 hours, both IR and PXRD spectra of the sample confirm that the structure of complex **2** can be remained well in the process of fluorescence experiment (Fig. S2 and S3†). Secondly, complex **2** exhibits excellent fluorescence sensing behaviors towards Fe^{3+}, MnO_4^-, CrO_4^{2-} and $Cr_2O_7^{2-}$ ions, and the quenching mechanism may be similar to those previous reports,[35,36] which was further confirmed by UV-vis spectra (Fig. S7†). Namely, both complexes and Fe^{3+}, MnO_4^-, CrO_4^{2-}, $Cr_2O_7^{2-}$ ions have overlap absorption bands in the 300–700 nm, which gives rise to the competition for excitation light absorption between the complexes and Fe^{3+}, MnO_4^-, CrO_4^{2-}, $Cr_2O_7^{2-}$ ions,[37] finally leading to the fluorescence quenching performance, which are similar to these previous reports.[38,39]

Optical band gaps and photocatalytic activity

As we know, many Co-based polyoxomolybdate-based metal organic framework exhibit usually good photocatalytic activities for the degradation of organic dyes under UV irradiation.[40–42] Therefore, in order to evaluate the semiconductor behaviors and photocatalytic activities of Co-based complex **1**, its diffuse reflection spectrum were measured in crystalline state at room temperature, as shown in Fig. 4. The band gap (E_g) of complex **1** is obtained by Kubelka–Munk (K–M) function,[43] where complex **1** is estimated at 2.00 eV. The results indicate that complex **1** can be used as potential semiconductor materials for photocatalytic reactions.[44]

The photocatalytic degradation activities of complex **1** for cationic dyes methylene blue (MB), neutral red (NR) and anionic dyes malachite green (MG), methyl orange (MO) were investigated here. The detail experimental operations were as follows: 50 mg of complex **1** was dispersed in 90 mL of a 0.02 mM aqueous solution containing different dyes. The mixtures were then stirred in the dark for about 30 minutes to ensure the adsorption–desorption equilibrium of the working solution. Next, the mixed solutions were continuously stirred under UV radiation, during which 4 mL samples were taken every 30

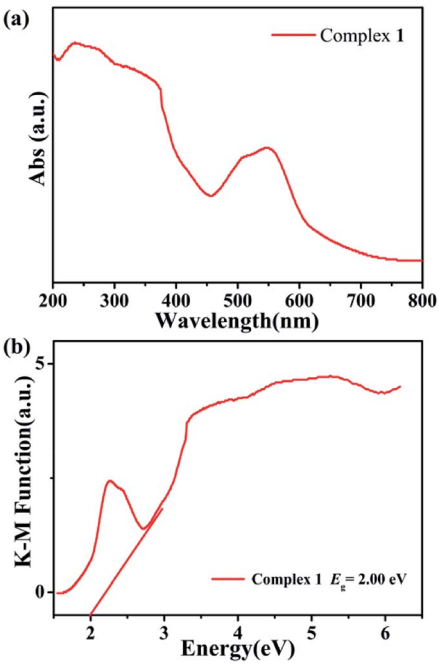

Fig. 4 (a) Diffuse-reflectance spectra (Abs) of complex **1**. (b) Diffuse reflection spectra of Kubelka–Munk (K–M) function *versus* energy (eV) of complex **1**.

minutes for MG and MO, 5 minutes for MB and NR, and analyzed by SP-1901 UV-vis spectrophotometer.[45]

As can be clearly shown in Fig. 5a and b, the absorption peaks of the cationic dyes (MB and NR) gradually decrease with the increase of UV irradiation time in the presence of complex **1** used as photocatalyst. After 30 minutes, the degradation rate reaches to as high as 93.6% for MB, 89.0% for NR, respectively. In contrast, no significant degradation towards anionic dyes MG and MO are observed at the same time, even after exposed to UV light for 150 minutes (Fig. 5c and d). Such catalytic efficiency is better than those in the previously reported literature. For example, Peter's group reported two new isostructural polyoxomolybdate-based metal organic complexes whose photocatalytic degradation efficiency for MB was 57% and 83%, respectively.[46]

The possible mechanism of the photocatalytic activity was derived as follows: POM was induced to shift from the highest occupied molecular orbital (HOMO) to the lowest unoccupied molecular orbital (LUMO) under UV irradiation. The excited state of POM* was generated during this period, accompanied by the formation of H^+, ·OH, and $\cdot O_2^-$, which can inactivate the organic dye during the oxidation process, thereby realizing the photocatalytic process.[47,48] In order to certificate the above mechanism, we introduced benzoquinone (BQ) as the quencher of $\cdot O_2^-$, isopropyl alcohol (IPA) as the quencher of ·OH, and triethanolamine (TEOA) as the quencher of H^+ to the photocatalytic MB and NR system. For the MB degradation reaction system, when IPA and TEOA were added separately, the photocatalytic degradation rate of complex **1** did not decrease significantly, and the presence of ·OH and H^+ was suppressed after the quencher being added, which indicates that ·OH and

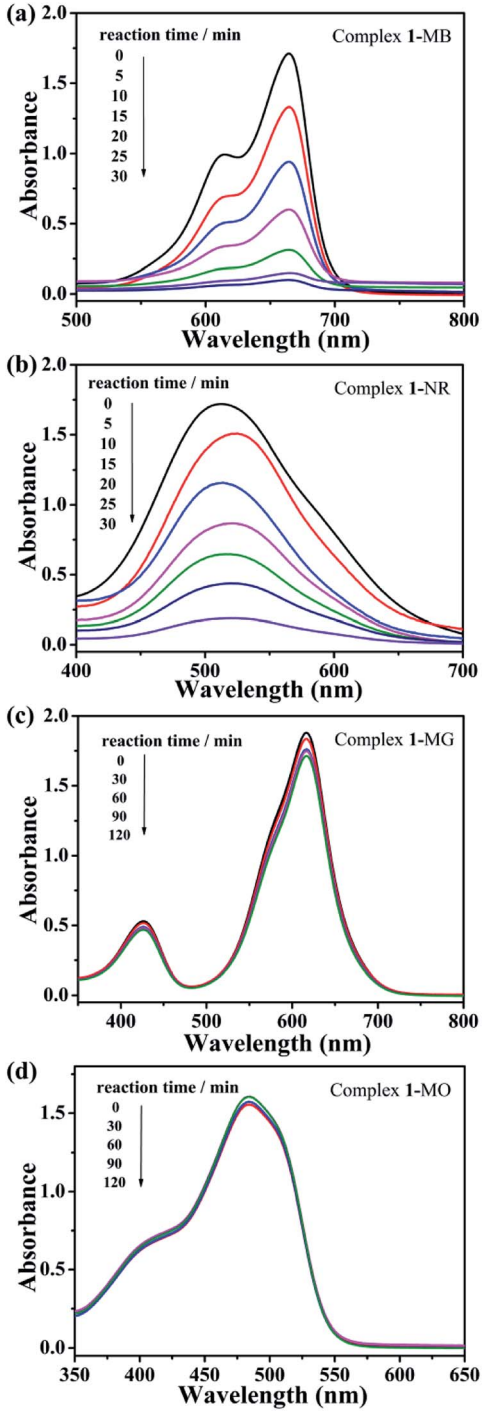

Fig. 5 (a) Absorption spectrum of MB, (b) NR, (c) MG and (d) MO solution during photocatalytic degradation reaction under UV radiation in the presence of complex **1**.

H^+ play a key role in the photocatalytic degradation of MB. After the addition of BQ, complex **1** can still effectively degrade MB, indicating that $\cdot O_2^-$ does not affect MB degradation (Fig. 6). As shown in Fig. S8,† in the NR degradation reaction system, the addition of BQ and IPA, respectively, did not reduced significantly the photocatalytic degradation rate of complex **1**, which

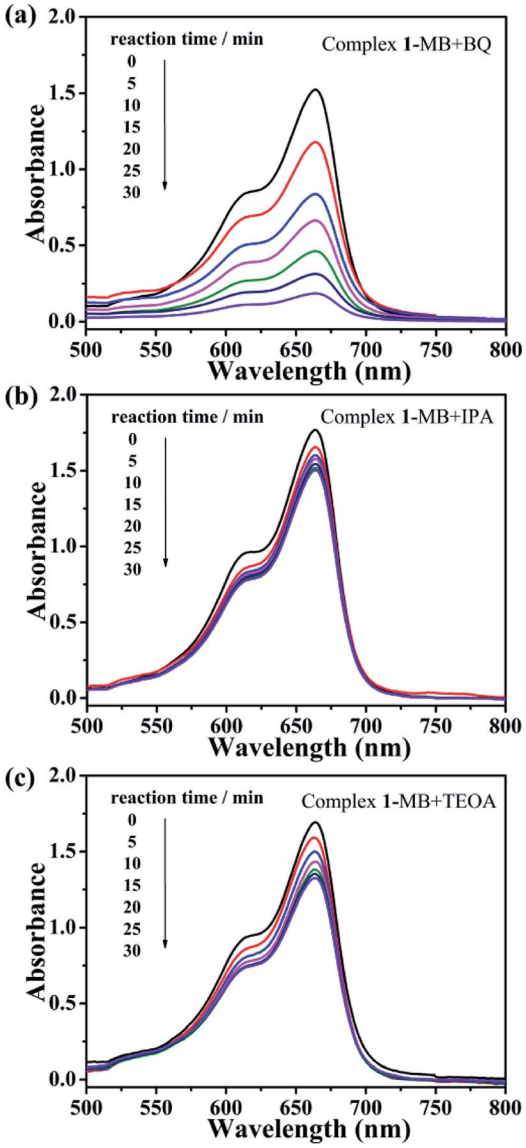

Fig. 6 Trapping experiments of active species (a) BQ, (b) IPA and (c) TEOA during the photocatalytic degradation MB reaction for complex **1**.

indicates that $\cdot O_2^-$ and $\cdot OH$ do appear and play a key role in oxidizing NR.

In addition, the stability of complex **1** during photocatalytic dye degradation was further measured. As shown in Fig. S2,† the PXRD spectra of both the experimental diffraction peaks of complex **1** after being used as photocatalyst and the simulated one are consistent, indicating that complex **1** is stable in photocatalytic experiments.[49] That is to say, complex **1** has excellent photocatalytic effect for the degradation of cationic dyes MB and NR under UV light, which may be good photocatalyst for degradation of the pollutants containing MB and NR.

Conclusions

In summary, we successfully synthesized two molybdate-based MOCs with bis-pyrazole-bis-amide ligand as organic linkers. A

kind of rare $\{M_2(MoO_4)_2\}_n$ (M = Co or Zn) chain in **1** and **2** were constructed from different raw materials. Two complexes have distinct performances because of different metal centers, **1** can be selected as fluorescent sensors for detecting Fe^{3+}, MnO_4^-, CrO_4^{2-} and $Cr_2O_7^{2-}$ ion, while **2** was better photocatalyst for degradation of cationic dyes MB and NR, which may be significant to exploit molybdate-based complexes with designated performance in the future.

Conflicts of interest

There are no conflicts to declare.

Acknowledgements

This work was financially supported by the National Natural Science Foundation of China (No. 21971024, 21671025 and 21771025) and supported by Liao Ning Revitalization Talents Program (XLYC1902011).

Notes and references

1 P. J. Zapf, D. Hagrman and J. Zubieta, *Angew. Chem., Int. Ed.*, 1999, **38**, 2638.
2 Q. F. Yang, J. Wang, X. Y. Chen, W. X. Yang, H. N. Pei, N. Hu, Z. H. Li, Y. R. Suo, T. Li and J. L. Wang, *J. Mater. Chem. A*, 2018, **6**, 2184.
3 L. Kan, J. Cai, Z. W. Jin, G. H. Li, Y. L. Liu and L. R. Xu, *Inorg. Chem.*, 2019, **58**, 391.
4 M. I. Khan, Q. Chen and J. Zubieta, *Inorg. Chim. Acta*, 1993, **213**, 325.
5 V. Damjanović, J. Pisk, D. Kuzman, D. Agustin, V. Vrdoljak, V. Stilinović and M. Cindrić, *Dalton Trans.*, 2019, **48**, 9974.
6 Y. R. Liu, J. X. Gou, X. Li, B. Dong, G. Q. Han, W. H. Hu, X. Shang, Y. M. Chai, Y. Q. Liu and C. G. Liu, *Electrochim. Acta*, 2016, **216**, 397.
7 L. Buzzetti, G. E. M. Crisenza and P. Melchiorre, *Angew. Chem., Int. Ed.*, 2019, **58**, 3730.
8 Y. Wang, X. P. Kong, W. Xu, F. R. Jiang, B. Li and L. X. Wu, *Inorg. Chem.*, 2018, **57**, 3731.
9 K. B. Wang, Z. K. Wang, S. E. Wang, Y. Chu, R. Xi, X. Y. Zhang and H. Wu, *Chem. Eng. J.*, 2019, **367**, 239.
10 D. Hagrman, C. J. Warren, R. C. Haushalter, C. Seip, C. J. O'Connor, R. S. Rarig, K. M. Johnson, R. L. LaDuca and J. Zubieta, *Chem. Mater.*, 1998, **10**, 3294.
11 A. X. Tian, Y. B. Fu, H. T. Cui, J. Ying, M. L. Yang, Y. Yang and X. L. Wang, *New J. Chem.*, 2019, **43**, 9980.
12 D. Hagrman and J. Zubieta, *Chem. Commun.*, 1998, 2005–2006.
13 D. J. Allis, R. S. Rarig, E. Burkholder and J. Zubieta, *J. Mol. Struct.*, 2004, **688**, 11.
14 R. S. Rarig, R. Lam, P. Y. Zavalij, J. K. Ngala, R. L. LaDuca, J. E. Greedan and J. Zubieta, *Inorg. Chem.*, 2002, **41**, 2124.
15 D. Hagrman, R. C. Haushalter and J. Zubieta, *Chem. Mater.*, 1998, **10**, 361.
16 C. Matthew Laskoski, L. Robert LaDuca, Jr., S. Randy Rarig, Jr. and J. Zubieta, *J. Chem. Soc., Dalton Trans.*, 1999, 3467.
17 C. Z. Lu, C. D. Wu, H. H. Zhuang and J. S. Huang, *Chem. Mater.*, 2002, **14**, 2649.
18 Y. Y. Guo, P. T. Ma, J. P. Wang and J. Y. Niu, *J. Solid State Chem.*, 2011, **184**, 3121.
19 V. V. Atuchin, A. S. Aleksandrovsky, B. G. Bazarov, J. G. Bazarova, O. D. Chimitova, Y. G. Denisenko, T. A. Gavrilova, A. S. Krylov, E. A. Maximovskiy, M. S. Molokeev, A. S. Oreshonkov, A. M. Pugachev and N. V. Surovtsev, *J. Alloys Compd.*, 2019, **785**, 692.
20 Y. B. Hua, S. K. Hussain and J. S. Yu, *New J. Chem.*, 2019, **43**, 10645.
21 M. Sarkar and K. Biradha, *Cryst. Growth Des.*, 2006, **6**, 202.
22 G. M. Sheldrick, *Acta Crystallogr., Sect. A: Found. Crystallogr.*, 2008, **64**, 112.
23 I. D. Brown and D. Altermatt, *Acta Crystallogr., Sect. B: Struct. Sci.*, 1985, **41**, 244.
24 S. Nam, A. D. French, B. D. Condon and M. Concha, *Carbohydr. Polym.*, 2016, **135**, 1.
25 S. Z. Ashraf, M. F. Erben and J. Simpson, *J. Mol. Struct.*, 2017, **1129**, 283.
26 J. Sárkány, *Appl. Catal., A*, 1999, **188**, 369.
27 Y. Shen, J. Peng, C. Y. Chen, H. Q. Zhang, C. L. Meng and X. L. Li, *Inorg. Chem. Commun.*, 2011, **14**, 221.
28 X. L. Wang, J. J. Sun, H. Y. Lin, Z. H. Chang, A. X. Tian, G. C. Liu and X. Wang, *Dalton Trans.*, 2016, **45**, 2709.
29 Y. Q. Lan, S. L. Li, X. L. Wang, K. Z. Shao, Z. M. Su and E. B. Wang, *Inorg. Chem.*, 2008, **47**, 529.
30 X. L. Wang, Y. Xiong, G. C. Liu, H. Y. Lin and X. Wang, *Dalton Trans.*, 2018, **47**, 9903.
31 L. N. Wang, Y. H. Zhang, S. Jiang and Z. Z. Liu, *CrystEngComm*, 2019, **21**, 4557.
32 G. C. Liu, Y. Li, J. Chi, N. Xu, X. L. Wang, H. Y. Lin and Y. Q. Chen, *Dyes Pigm.*, 2020, **174**, 108064.
33 C. B. Yang, C. B. Jiang, M. Y. Zhang, X. Chen, P. Zou, R. W. Yang, H. B. Rao and G. T. Wang, *Polyhedron*, 2020, **175**, 114216.
34 Y. Q. Chen, Y. Tian, S. L. Yao, J. Zhang, R. Y. Feng, Y. J. Bian and S. J. Liu, *Chem.–Asian J.*, 2019, **14**, 4420.
35 L. Wang, W. Xu, W. Y. Li, M. Xie and Y. Q. Zheng, *Chem.–Asian J.*, 2019, **14**, 4246.
36 Q. Q. Xiao, G. Y. Dong, Y. H. Li and G. H. Cui, *Inorg. Chem.*, 2019, **58**, 15696.
37 X. S. Li, J. D. An, H. M. Zhang, J. J. Liu, Y. Li, G. X. Du, X. X. Wu, L. Fei, J. D. Lacoste, Z. Cai, Y. Y. Liu, J. Z. Huo and B. Ding, *Dyes Pigm.*, 2019, **170**, 107631.
38 L. Wang, T. T. Guo, J. C. Ma, Y. Y. Liu, G. H. Xu and J. F. Ma, *ChemistrySelect*, 2019, **4**, 7351.
39 W. Q. Kan and S. Z. Wen, *Dyes Pigm.*, 2017, **139**, 372.
40 A. X. Tian, J. N. Liu, X. B. Ji, G. Y. Liu, T. T. Li, Y. Tian, H. P. Ni, G. C. Liu and J. Ying, *J. Mol. Struct.*, 2018, **1155**, 371.
41 H. Ramezanalizadeh and F. Manteghi, *J. Photochem. Photobiol., A*, 2017, **346**, 89.
42 X. Pan, X. L. Wang, X. Wang, Y. Li, G. C. Liu and H. Y. Lin, *CrystEngComm*, 2019, **21**, 6472.
43 H. J. Du, C. H. Wang, Y. Li, Y. Y. Niu and H. W. Hou, *RSC Adv.*, 2015, **5**, 74065.

44 H. Y. Liu, L. Bo, J. Yang, Y. Y. Liu, J. F. Ma and H. Wu, *Dalton Trans.*, 2011, **40**, 9782.
45 X. L. Wang, R. Zhang, X. Wang, H. Y. Lin, G. C. Liu and H. X. Zhang, *Dalton Trans.*, 2017, **46**, 1965.
46 S. Roy, V. Vemuri, S. Maiti, K. S. Manoj, U. Subbarao and S. C. Peter, *Inorg. Chem.*, 2018, **57**, 12078.
47 X. X. Zhao, S. W. Zhang, J. Q. Yan, L. D. Li, G. J. Wu, W. Shi, G. M. Yang, N. J. Guan and P. Cheng, *Inorg. Chem.*, 2018, **57**, 5030.
48 S. M. Wang, D. L. Li, C. Sun, S. G. Yang, Y. Guan and H. He, *Appl. Catal., B*, 2014, **144**, 885.
49 X. L. Wang, R. Zhang, X. Wang, H. Y. Lin and G. C. Liu, *Inorg. Chem.*, 2016, **55**, 6384.